Received: 3 December 2020 | Revised: 18 January 2021 | Accepted: 13 February 2021

DOI: 10.1002/htj.22102

RESEARCH ARTICLE

HEAT TRANSFER WILEY

The effect of Joule heating and viscous dissipation on the boundary layer flow of a magnetohydrodynamics micropolar-nanofluid over a stretching vertical Riga plate

Nabil T. Eldabe[1] | **Mahmoud E. Gabr**[2] | **Abdullah Z. Zaher**[3] | **Sameh A. Zaher**[2]

[1]Department of Mathematics, Faculty of Education, Ain Shams University, Cairo, Egypt

[2]Department of Mathematics, Faculty of Science, Zagazig University, Zagazig, Egypt

[3]Department of Engineering Mathematics and Physics, Faculty of Engineering, Shubra-Benha University, Banha, Egypt

Correspondence
Sameh A. Zaher, Department of Mathematics, Faculty of Science, Zagazig University, 44519 Zagazig, Egypt.
Email: samehabdelzaher419@yahoo.com

Abstract

Joule heating and viscous dissipation effects on the behavior of the boundary layer flow of a micropolar nanofluid over a stretching vertical Riga plate (electro magnetize plate) are considered. The flow is disturbed by an external electric magnetic field. The problem is formulated mathematically by nonlinear system of partial differential equations (PDEs). By using suitable variables transformations, this system is transformed onto a system of nonlinear ordinary differential equations (ODEs). The Parametric NDsolve package of the commercial software Mathematica is used to solve the obtained ODEs as well as the considered numerical results for different physical parameters with appropriate boundary conditions. Novel results are obtained by studying the stream lines flow around the plate in two and three dimensions. Moreover, the effects of the pertinent parameters on the skin friction coefficient, couple stress, local Nusselt, and Sherwood number are discussed. Special cases of the obtained results show excellent agreements with previous works. The results showed that as the magnetic field parameter increases the velocity of the boundary layer adjacent to the stretching sheet

decreases. Also, for a productive chemical reaction near the sheet surface, the angular velocity decreases but opposite trend is observed far from the sheet surface. The importance of this study comes from its significant applications in many scientific fields, such as nuclear reactors, industry, medicine, and geophysics.

KEYWORDS
boundary layer, computational solution, magnetohydrodynamics, micropolar fluids, Riga plate, stream lines flow

1 | INTRODUCTION

The importance of studying nanofluids behavior under the effect of different external forces comes from its wide applications in different engineering industries. Nanofluids have different physical and chemical properties depending on its nanoparticles. In some specific fluids, the suspension of nanosized particles improve significantly fluid properties, such as thermal conductivity, thermal diffusivity, viscosity, and heat transfer convective. The term Nanofluid refers to Choi[1] and Choi et al.[2] they proved that when small amounts of nanoparticles added to the base fluid increases the fluid thermal conductivity to at least twice time its thermal prosperity. Nanoparticles such as aluminum, copper, iron, and titanium when added to a nanofluid change its physical and chemical properties differently, especially the thermal conductivity of these substances.

In the last few decades, many scientists devoted their attention to study the nanofluid's thermal properties, assuming different external fields. Recently, Reddy et al.[3] analyzed the effect of Prandtl non-Newtonian nanofluid on Zero-mass flux and Cattaneo–Christov heat flux through a Darcy–Forchheimer porous space. They found that for larger thermophoretic force constraint and Brownian movement factor the thermal field is boosted. Also, improving the thermophoretic and Brownian movement parametric values leads to higher profile of Prandtl nanofluid temperature. Shehzad et al.[4] utilized the Catano–Christov double diffusion theories to study fluid motion caused by a rotating stretched disk. Reddy et al.[5] presented numerical study to investigate the impact of magnetic field and Ohmic heating on the flow of a viscous dissipative nanofluid with heat transfer, in the presence of porous medium, through a nonlinearly stretching sheet.

Because of the recent revaluation in engineering industries as well as the development of many classical fluids into nanofluids, the need for scientists and engineers to study the microstructures of these fluids is now a huge challenge. The theory of Eringen is commonly used to study these kinds of fluids, where the deformation of the fluid rigid bodies is included. Examples of such fluids are polymeric suspensions, biological fluids, liquid crystals with stiff molecules, muddy fluids, and nemotogenic and semectogenic liquids crystals. These fluids are models of fluids that contain small, randomly oriented particles, suspended in a viscous medium. These rigid particles' motion consists of both translational and rotational motion. Often, spin inertia determines the stress moments and body pairs, in addition the stress tensor

is not symmetric. This is a good mathematical model for many natural and industrial fluids, such as blood flow, lubricants, turbulent shear flows, and flow in capillaries, and microchannels.

Eringen[6,7] developed the concept of micropolar fluids by studying the effects of microrotation of the fluid microstructures. Arafa and Gorla[8] performed a study for buoyancy and curvature convection in micropolar fluids flow through vertical cylinders with needles and concluded that the fluid microrotation is significantly enhanced when considering nonhomogeneous boundary conditions. Nadeem et al.[9] investigated the same problem by considering the flow of a micropolar nanofluid in a moving cylinder with finite radius and concluded that increasing the micropolar parameter value the velocity, angular velocity, and surface temperature are also increase. Bourantas and Loukopoulos[10] presented a natural convection study of a micropolar nanofluid (Al_2O_3) along a rectangular inclined enclosure. The mixed convection flow of a micropolar nanofluid near a stagnation point past a vertical stretch sheet was discussed by Noor et al.[11] Rehman and Nadeem[12] indicated that the pertinence of the boundary layer theory to the hybrid convection flow of micropolar nanofluid in a vertical slender cylinder. It was shown that as the micropolar parameter increases the velocity and temperature of the fluid at the boundary decrease. Ram Reddy et al.[13] investigated the solution of similarity for stable free flow of micropolar fluids convections through a convective boundary vertical surface.

Besides its significant effects on conductivity structure and dynamics of micropolar fluids, magnetic field also disturbs the fluid flow. These effects are due to the induced Lorentz force as a result of magnetic flux changes. Many engineering applications considered Lorentz force, where magnetohydrodynamic (MHD) flows are encountered such as Fridge, nuclear reactors, and MHD accelerators. The mathematical formulation of these kinds of flow is very complicated due to the additional MHD equations. Besthapu et al.[14] addressed the impact of thermally stratified nanofluid by considering the impact of buoyancy on a spongy stretching surface. Ramzan et al.[15] determined the optimal solution of Maxwell nanofluid flow problem. For more important and significant results for the effect of nanoparticles and how it improves the thermal conductivity of nanofluids see also References [16-21].

The main goal of this paper is to study the electrically conducting micropolar nanofluid on steady electromagnetohydrodynamic (EMHD)-free convection and mass transfer flow over a stretching vertical Riga plate (electro magnetize plate). After using special similarity transformation, the governing equations of the problem transformed into an ordinary coupled system of nonlinear ordinary differential equations. With the help of the Parametric NDsolve package of the commercial software Mathematica, this system is solved numerically. Important numerical results for different physical parameters with appropriate boundary conditions are obtained. Two- and three-dimension representations for the stream lines around the plate is introduced with physical explanations as well as the others obtained results.

2 | FORMULATION OF THE PROBLEM

Consider a two-dimensional steady flow of an incompressible micropolar nanofluid over a linearly stretching vertical Riga plate. The flow is disturbed by a uniform magnetic field, $\underline{B} = (0, B_O, 0)$ acting normally on the flow direction for small magnetic Reynolds number. Moreover, the fluid is electrically conducting by an electric field $\underline{E} = (0, 0, -E_0)$, and both the magnetic and electric fields obeying Ohm's law $\underline{J} = \sigma(\underline{E} + \underline{V} \times \underline{B})$, where $\underline{J}$, σ, and $\underline{V}$ are the Joule current, the electrical conductivity, and the velocity filed, respectively. When considering

small magnetic Reynolds number, the induced magnetic field may be ignored. The governing equations of the fluid boundary layer flow of the considered problem are the continuity equation, the momentum equation, the angular momentum equation, the energy equation, and the concentration equation. Also, the laws of Maxwell and Ohm should be considered during this formulation.

Using Buongiorno's model,[22,23] the governing equations can be written as

The continuity equation:

$$\nabla\cdot\vec{V} = 0. \tag{1}$$

The momentum equation:

$$\rho_f\left(\frac{\partial\vec{V}}{\partial t} + (\vec{V}\cdot\nabla)\vec{V}\right) = -\nabla P + k_1(\nabla\times\vec{N}) + (\mu + k_1)\nabla^2\vec{V} + \vec{J}\times\vec{B} + \vec{F} + \{\beta_T(T - T_\infty) + \beta_C(C - C_\infty)\}\vec{g}. \tag{2}$$

The angular momentum equation:

$$\rho_f j\left(\frac{\partial\vec{N}}{\partial t} + (\vec{V}.\ \nabla)\vec{N}\right) = -2k_1\vec{N} + k_1(\nabla\times\vec{V}) - \gamma^*(\nabla\times(\nabla\times\vec{N})) + (\alpha^* + \beta^* + \gamma^*)\nabla(\nabla.\ \vec{N}). \tag{3}$$

The energy equation:

$$(\rho c)_f\left(\frac{\partial T}{\partial t} + (\vec{V}\cdot\nabla)T\right) = k_r\nabla^2 T + (\rho c)_p\left\{D_B\nabla C\cdot\nabla T + \left(\frac{D_T}{T_\infty}\right)\nabla T\cdot\nabla T\right\} + \frac{\left(\vec{J}.\ \vec{J}\right)}{\sigma} + \vec{\tau}\cdot\nabla\vec{V}. \tag{4}$$

The concentration equation:

$$\left(\frac{\partial C}{\partial t} + (\vec{V}\cdot\nabla)C\right) = D_B\nabla^2 C + \left(\frac{D_T}{T_\infty}\right)\nabla^2 T + k_o(C - C_\infty). \tag{5}$$

3 | BASIC EQUATIONS

Choose the Cartesian coordinate (x, y, z) and let the plan $y = 0$ represents the infinite stretching sheet. Let $u(x, y)$ and $v(x, y)$ be the components of the velocity field (Figure 1). Based on the standard boundary layer approximation, the two-dimensional EMHD boundary layer flow equations for the considered incompressible micropolar nanofluid are:

The continuity equation:

$$\frac{\partial u}{\partial x} + \frac{\partial v}{\partial y} = 0. \tag{6}$$

The momentum equation:

$$u\left(\frac{\partial u}{\partial x}\right) + v\left(\frac{\partial u}{\partial y}\right) = \frac{(\mu + k_1)}{\rho_f}\frac{\partial^2 u}{\partial y^2} + \frac{k_1}{\rho_f}\left(\frac{\partial N^*}{\partial y}\right) + \frac{\sigma}{\rho_f}(E_o B_o - B^2{}_o u) + \frac{nM_o j_o}{8\rho_f}\exp\left(-\frac{\pi}{a}y\right) + g\beta_T(T - T_\infty) + g\beta_C(C - C_\infty). \tag{7}$$

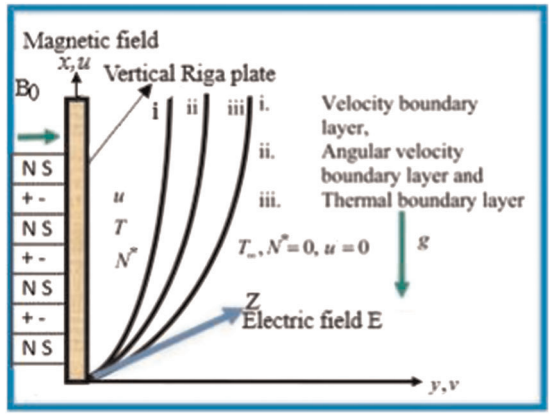

FIGURE 1 Physical configuration of the geometry [Color figure can be viewed at wileyonlinelibrary.com]

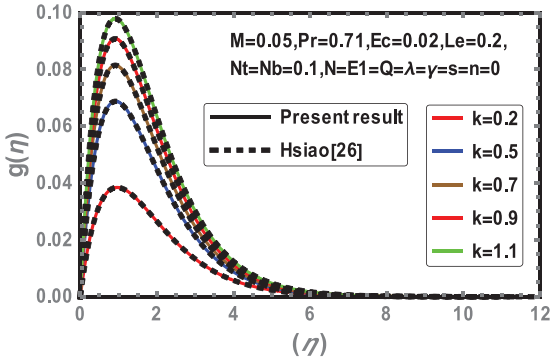

FIGURE 2 Comparison of angular velocity distribution with Hsiao[26] [Color figure can be viewed at wileyonlinelibrary.com]

The angular momentum equation:

$$\rho_f j\left(u\frac{\partial N^*}{\partial x}+v\frac{\partial N^*}{\partial y}\right)=\gamma^*\frac{\partial^2 N^*}{\partial y^2}-k_1\left(2N^*+\frac{\partial u}{\partial y}\right). \tag{8}$$

The energy equation:

$$u\frac{\partial T}{\partial x}+v\frac{\partial T}{\partial y}=\alpha\frac{\partial^2 T}{\partial y^2}+\tau_1\left[D_B\frac{\partial c}{\partial y}\frac{\partial T}{\partial y}+\frac{D_T}{T_\infty}\left(\frac{\partial T}{\partial y}\right)^2\right]+\frac{(\mu+k)}{(\rho c)_f}\left(\frac{\partial u}{\partial y}\right)^2+\frac{\sigma}{(\rho c)_f}(B_o u-E_o)^2. \tag{9}$$

The concentration equation:

$$u\frac{\partial C}{\partial x}+v\frac{\partial C}{\partial y}=D_B\frac{\partial^2 C}{\partial y^2}+\frac{D_T}{T_\infty}\left(\frac{\partial^2 T}{\partial y^2}\right)+k_\circ(C-C_\infty). \tag{10}$$

where, k_1 is the vortex viscosity coefficient, N^* is the component of the microrotation vector $\vec{N}$ normal to the x and y-axes, and j is the micro inertia density.

The spin gradient γ^* can be defined as

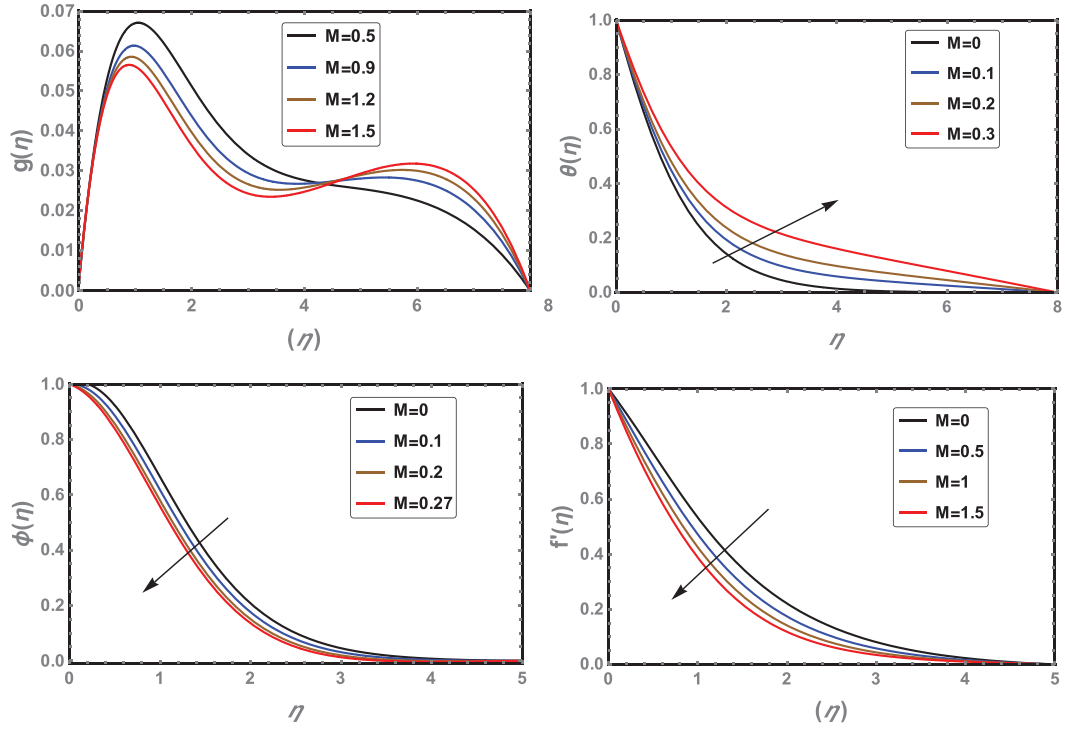

FIGURE 3 The variation of magnetic field on $f'(\eta)$, $\phi(\eta)$, $g(\eta)$, and $\theta(\eta)$ [Color figure can be viewed at wileyonlinelibrary.com]

$$\gamma^* = \left(\mu + \frac{k_1}{2}\right)j = \mu\left(1 + \frac{K}{2}\right)j, \tag{11}$$

where $K = \frac{k_1}{\mu}$ is the material parameter, $j = \frac{\upsilon_f}{c}$ is the micro inertia constant.

The boundary conditions are as follows:

$$y = 0: \quad v = v_w, \quad u = U_w(x) = cx, \quad N^* = -n\frac{\partial u}{\partial y}; \quad T = T_w, \quad C = C_w, \quad N = N_w, \quad y \to \infty: \quad u \to 0, \quad N^* \to 0, \quad C \to C_\infty, \quad T \to T_\infty, \quad N \to N_\infty, \tag{12}$$

where, c is the surface stretching constant and v_W its velocity.

4 | METHOD OF SOLUTION

To solve the system of partial differential Equations (7)–(10) subject to the boundary conditions (12), we use the following similarity transformations[24]:

$$\psi = (c\upsilon)^{\frac{1}{2}}xf(\eta), \quad \theta(\eta) = \frac{T - T_\infty}{T_w - T_\infty}, \quad \phi(\eta) = \frac{C - C_\infty}{C_w - C_\infty}; \quad \eta = y\left(\frac{c}{\upsilon}\right)^{\frac{1}{2}}, \quad N = c\left(\frac{c}{\upsilon}\right)^{\frac{1}{2}}xg(\eta), \tag{13}$$

where $\psi(x, y)$ is the stream function such that $u = \frac{\partial \psi}{\partial y}$ and $v = -\frac{\partial \psi}{\partial x}$.

The transformation (13) identically satisfies the continuity equation.

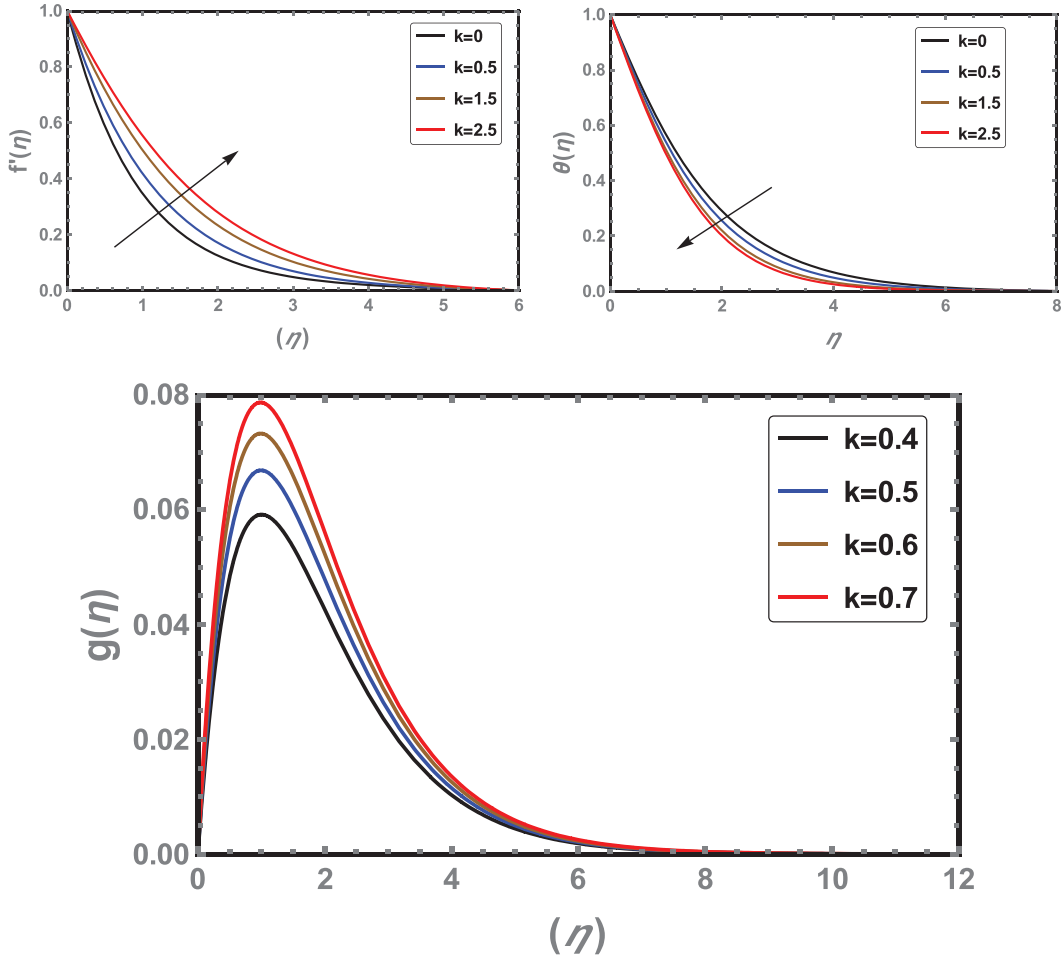

FIGURE 4 The variation of material parameter K on $f'(\eta)$, $\phi(\eta)$, $g(\eta)$, and $\theta(\eta)$ [Color figure can be viewed at wileyonlinelibrary.com]

Introducing this transformation into the governing Equations (6-10) and the boundary conditions (12), we obtain the following nonlinear coupled system of ordinary differential equations:

The momentum equation

$$(1+K)f'''(\eta)+f(\eta)f''(\eta)-(f'(\eta))^2+Qexp(-A\eta)+Kg'(\eta)+M(E_1-f'(\eta)) + \lambda(\theta(\eta)+N\phi(\eta))=0. \tag{14}$$

The angular momentum equation

$$\left(1+\frac{K}{2}\right)g''(\eta)+f(\eta)g'(\eta)-f'(\eta)g(\eta)-K(2g(\eta)+f''(\eta))=0. \tag{15}$$

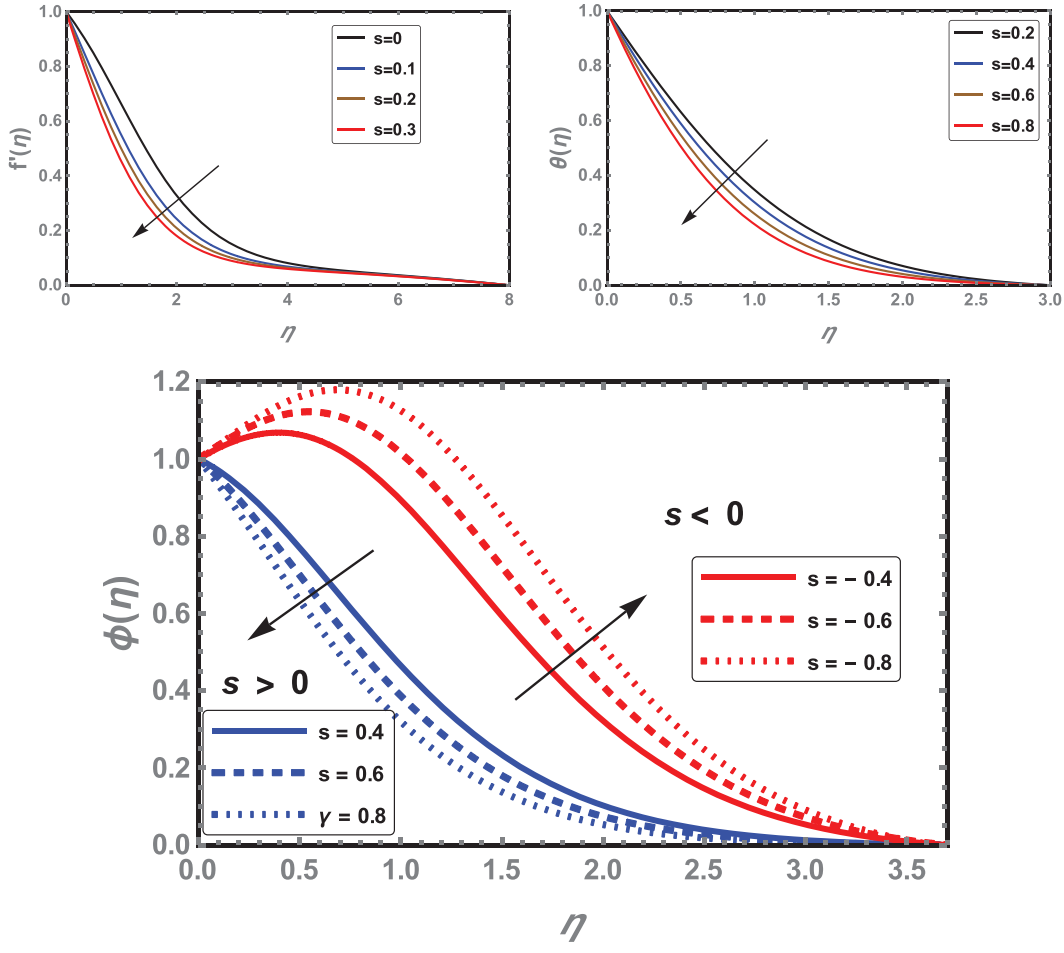

FIGURE 5 The variation of parameter of suction (s) on $f'(\eta)$, $\phi(\eta)$, $g(\eta)$, and $\theta(\eta)$ [Color figure can be viewed at wileyonlinelibrary.com]

The energy equation

$$\frac{1}{p_r}\theta''(\eta) + f(\eta)\theta'(\eta) + N_b\theta'(\eta)\phi'(\eta) + N_t\theta'(\eta)^2 + E_c(1+K)(f''(\eta))^2 + ME_c(f'(\eta) - E_1)^2 = 0. \tag{16}$$

The concentration equation

$$\phi''(\eta) + \frac{N_t}{N_b}\theta''(\eta) + L_e f(\eta)\phi'(\eta) + L_e\gamma\phi(\eta) = 0. \tag{17}$$

The boundary conditions:

$$f(0) = s,\ f'(0) = 1,\ g(0) = -nf''(0),\ \theta(0) = 1,\ \Phi(0) = 1,\ \text{at}\ \eta = 0;$$
$$f'(\eta) \to 0,\ g(\eta) \to 0,\ \theta(\eta) \to 0,\ \Phi(\eta) \to 0:\ \text{at}\ \eta \to \infty. \tag{18}$$

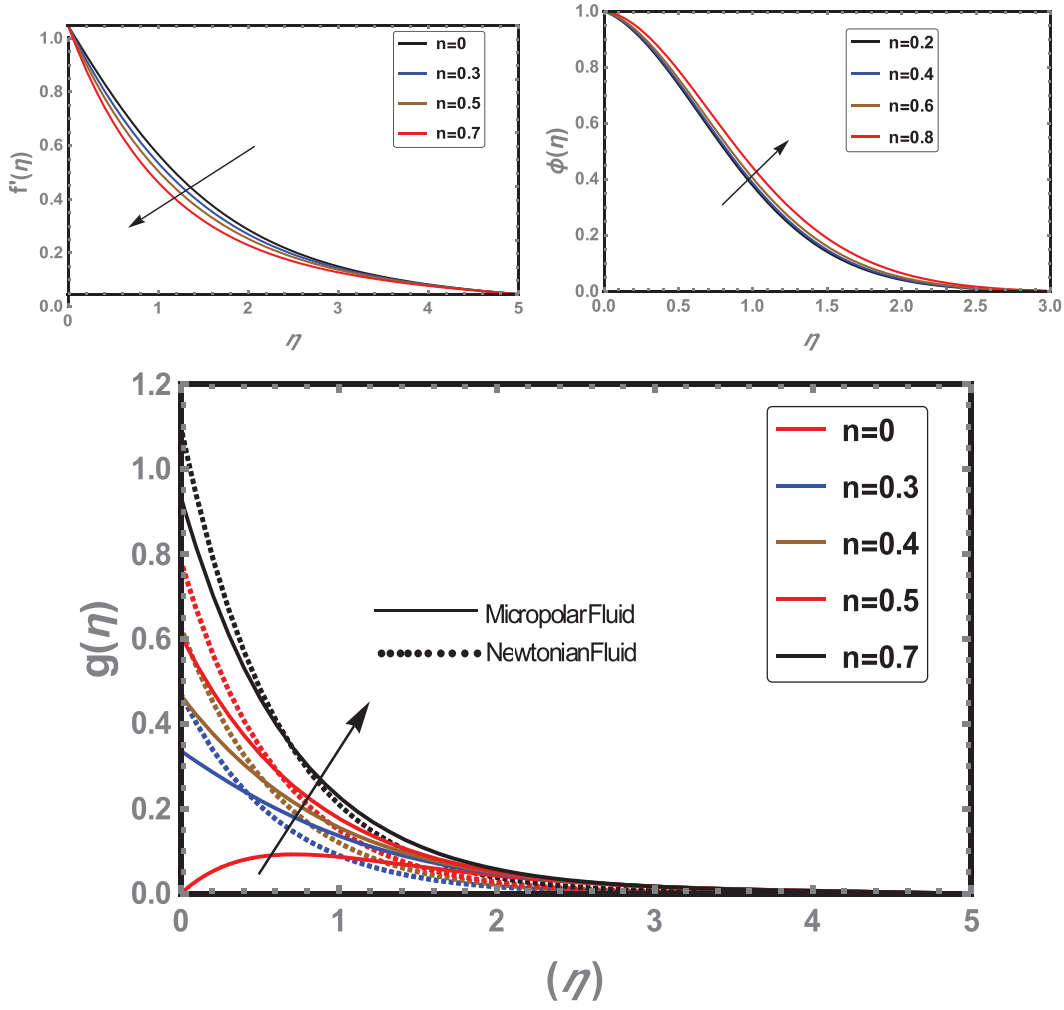

FIGURE 6 The variation of boundary parameter on $f'(\eta)$, $\phi(\eta)$, $g(\eta)$, and $\theta(\eta)$ [Color figure can be viewed at wileyonlinelibrary.com]

where, the dimensionless variables f, θ, g, and ϕ represent the velocity, temperature, angular velocity (microrotation), and concentration, respectively.

The parameters are defined as follows:

$$M = \frac{\sigma {B_O}^2}{c\rho_f},\quad E_1 = \frac{E_0}{cxB_0},\quad \lambda = \frac{G_{rx}}{{R^2}_{ex}},\quad G_{rx} = \frac{G\beta_T(T_W - T_\infty)x^3}{\upsilon^2},\quad R_{ex} = \frac{u_w(x)x}{\upsilon},$$

$$Q = \frac{\pi M_o j_o}{8c^2 x\rho_f},\quad A = \frac{\pi}{a}\sqrt{\frac{\upsilon}{c}},\quad {G^*}_{rx} = \frac{G\beta_c(C_W - C_\infty)x^3}{\upsilon^2},\quad N = \frac{{G^*}_{rx}}{G_{rx}},\quad pr = \frac{\upsilon}{\alpha},$$

$$Nb = \frac{(\rho c)_p D_B(C_w - C_\infty)}{(\rho c)_f \upsilon},\quad Nt = \frac{(\rho c)_p D_T(T_w - T_\infty)}{T_\infty(\rho c)_f \upsilon},\quad Le = \frac{\upsilon}{D_B},\quad \gamma = \frac{k_0}{c},$$

$$E_c = \frac{u_w^2}{c_p(T_w - T_\infty)}.$$

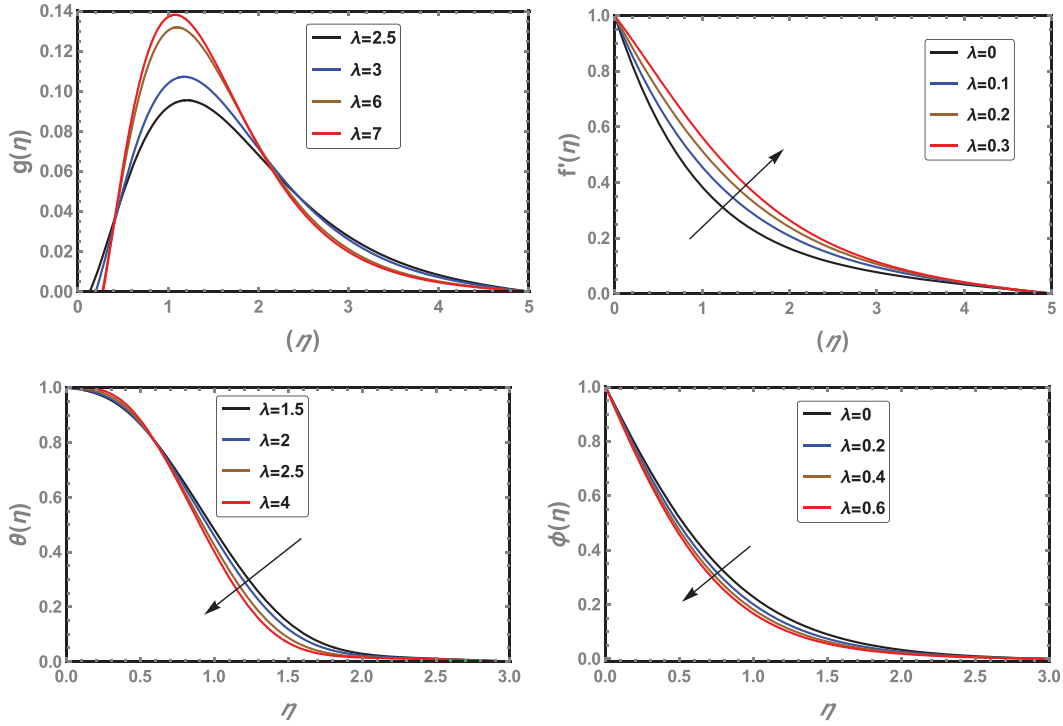

FIGURE 7 The variation of mixed convection parameter λ on $f'(\eta)$, $\phi(\eta)$, $g(\eta)$, and $\theta(\eta)$ [Color figure can be viewed at wileyonlinelibrary.com]

The mathematical formulas of the Nusselt number (Nu), Sherwood number (Sh), couple stress at the surface (M_w), and skin friction coefficient (c_f) are

$$Nu = \frac{xq_w}{k_f(T_w - T_\infty)}, \quad sh = \frac{xq_m}{D_B(C_W - C_\infty)}, \quad M_w = \left(\gamma^* \frac{\partial N^*}{\partial y}\right)_{y=0}, \quad c_{fx} = \frac{\tau_w}{\rho_f u_w^2(x)}. \tag{19}$$

The wall heat and mass flux q_w and q_m and the wall shear stress τ_w are

$$q_w = -k_f\left(\frac{\partial T}{\partial y}\right)_{y=0}, \quad q_m = -D_B\left(\frac{\partial C}{\partial y}\right)_{y=0}, \quad \tau_w = (\mu + k)\left(\frac{\partial u}{\partial y}\right)_{y=0} + kN^*(y)_{y=0}. \tag{20}$$

Inserting Equation (14) in (15) we obtain:

$$-\theta'(0) = \sqrt{\frac{1}{R_{ex}}}Nu_x, \quad -\Phi'(0) = \sqrt{\frac{1}{R_{ex}}}Sh_x, \quad M_w = uu_w\left(1 + \frac{K}{2}\right)g'(0),$$
$$c_f = \sqrt{\frac{1}{R_{ex}}}\left[(1-n)Kf''(0) + f''(0)\right], \tag{21}$$

where $R_{ex} = \frac{ux}{\upsilon}$ is the local Reynolds number.

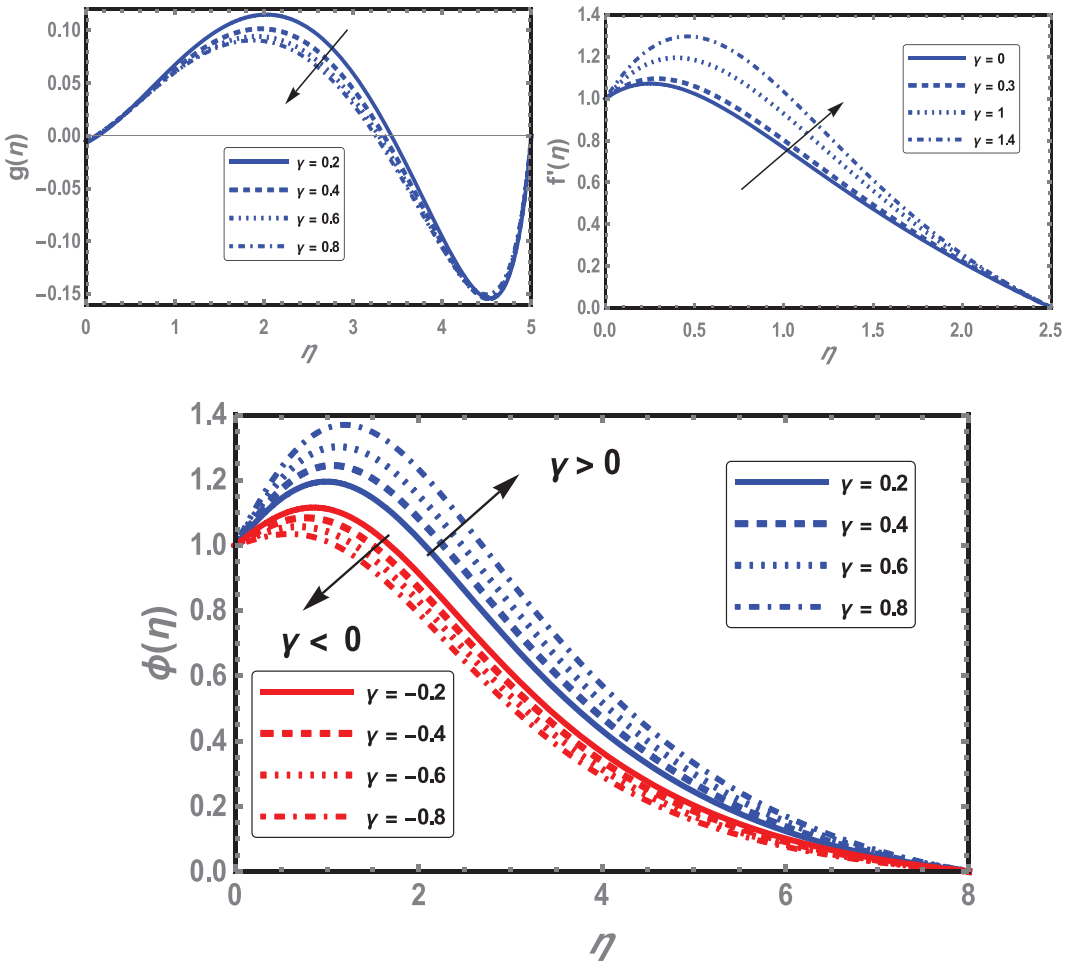

FIGURE 8 The variation of chemical reaction parameter γ on $f'(\eta)$, $\phi(\eta)$, and $g(\eta)$ [Color figure can be viewed at wileyonlinelibrary.com]

5 | RESULTS AND DISCUSSION

In the present work, the electrically conducting micropolar nanofluid MHD with heat and mass transfer flow over a stretching vertical Riga plate is investigated, as well as the viscous dispersion, Ohmic heating, and chemical reaction. The Parametric NDsolve package of the commercial software Mathematica is used to obtain the numerical solution of the problem nondimensional system of ordinary differential equations with suitable boundary conditions.

Tables 1 and 2 contain comparison between the results of the present problem and previous works. Complete agreement is proved with the works of Eldabe et al.[25] and Hsiao[26] (Eldabe et al. chose $Pr = 0.71, Ec = 0.02, Le = 0.2, Nt = Nb = \gamma = n = s = Q = \lambda = E_1 = N = 0$ and Hsiao chose $M = 0.05, Nt = Nb = 0.1, Pr = 0.71, Ec = 0.02, Le = 0.2, \gamma = n = s = Q = \lambda = E_1 = N = 0$). Table 3 shows the results of some physical values, such as skin friction coefficient, couple stress, local Nusselt, and Sherwood number for larger values of K, λ, Pr, and E_1. As a result of this, we conclude that couple stress $g'(0)$ and local Nusselt number $-\theta'(0)$ increased, while skin friction coefficient and Sherwood number decreased. The main results of the present work are given in Figures 3-11.

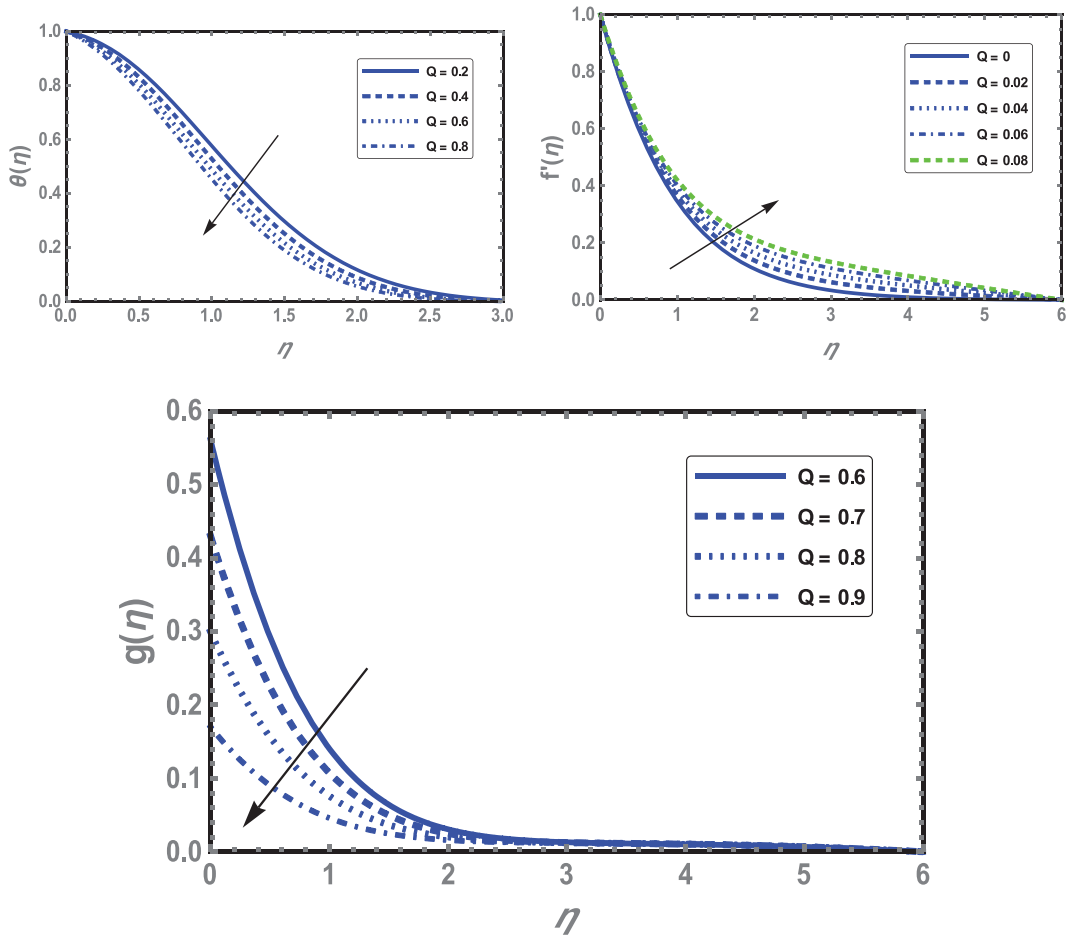

FIGURE 9 The variation of modified Hartman number Q on $f'(\eta)$, $g(\eta)$, and $\theta(\eta)$ [Color figure can be viewed at wileyonlinelibrary.com]

The numerical results for material parameter on angular velocity distribution are presented in Figure 2 in the case of $(M = 0.05, Nt = Nb = 0.1, Pr = 0.71, Ec = 0.02, Le = 0.2, \gamma = n = s = Q = \lambda = E_1 = N = 0)$ as a comparison with Hsiao.[26]

Figure 3 demonstrate the behavior of the velocity $f'(\eta)$, angular velocity $g(\eta)$, temperature $\theta(\eta)$, and concentration $\phi(\eta)$ for certain values of the magnetic field parameter M. As a result of the induced Lorentz force, increasing the magnetic field increases $\theta(\eta)$, and decreases $f'(\eta)$, $\phi(\eta)$, and (η). The behavior of $f'(\eta)$, $\phi(\eta)$, $g(\eta)$, and $\theta(\eta)$are shown in Figure 4 under the effect of material parameter K. It is shown that with increasing material parameter K $f'(\eta)$ and $g(\eta)$, increases but $\theta(\eta)$ decreases. Figure 4 indicates the effect of the material number K. We noticed that increasing the material parameter rapidly increases the angular velocity. The momentum of the flow field can be increased by the obtained material force. On the other hand, the physical processes of temperature have the opposite effects.

Figure 5 displays the effects of suction and injection parameter (s) on the velocity $f'(\eta)$, concentration $\phi(\eta)$, and temperature profiles $\theta(\eta)$. These variables decrease with the increase of suction and injection parameter. The increases in the viscous force is due to the resistance force caused by the diffusion of the heated fluid through the plate.

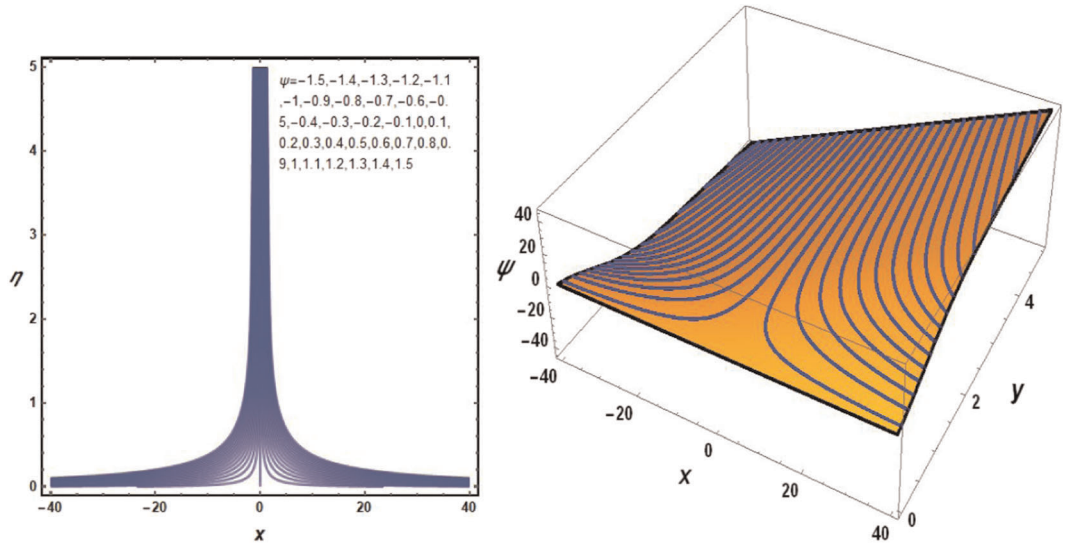

FIGURE 10 Streamlines for $E_1 = 1.5$ [Color figure can be viewed at wileyonlinelibrary.com]

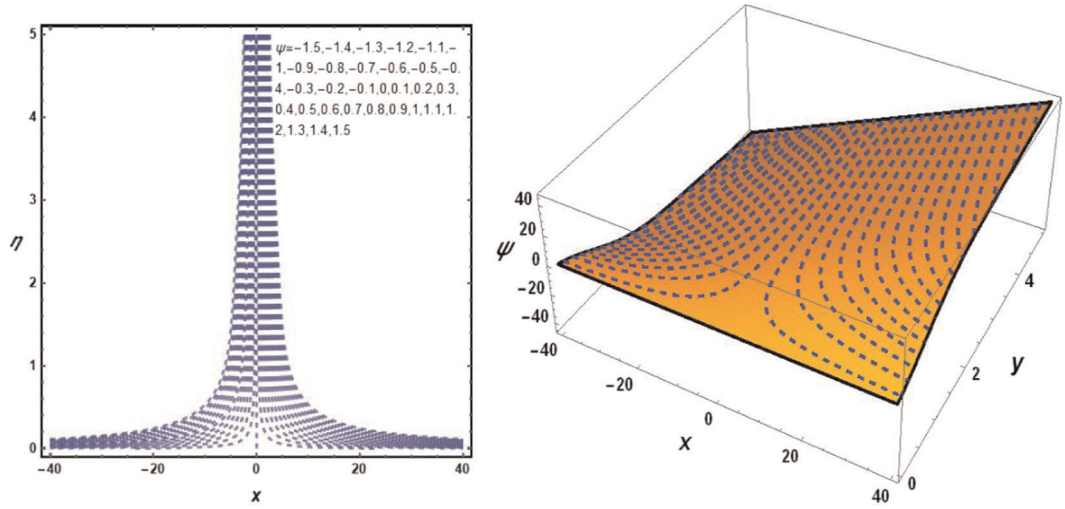

FIGURE 11 Streamlines for $E_1 = 0.5$ [Color figure can be viewed at wileyonlinelibrary.com]

In Figure 6, we present a comparison study between Newtonian fluid and micropolar fluid (which is considered in non-Newtonian fluid) under the effect of boundary parameter. For a Newtonian fluid, choose $K = 0$ in Equation (9). The study showed that, significant increases in the micropolar fluid velocity as well as its microrotation but decreases its concentration.

Figure 7 displays the behavior of mixed convection parameter λ on the fluid velocity $f'(\eta)$ and microrotation profiles $g(\eta)$. We notice that increasing the mixed convection parameter λ increases the fluid velocity and microrotation profiles. For large values of λ, the temperature $\theta(\eta)$ and concentration $\phi(\eta)$ decrease. This is because the amount of local Grashof number G_{rx} reflects the buoyancy to viscous force ratio. Any increase in G_{rx} obviously contributes to an

TABLE 1 Comparison of the couple stress at the surface $g'(0)$ and the skin friction coefficient $-f''(0)$ versus K and M of the present study with that of Eldabe et al.[25] and Hsiao[26]

		$g'(0)$			$-f''(0)$		
M	K	Ref. [25]	Ref. [26]	Present	Ref. [25]	Ref. [26]	Present
0.0	0.2	0.0950	0.0950	0.0950	0.9098	0.9098	0.9098
0.5	0.2	0.1051	0.1051	0.1051	1.1148	1.1147	1.1144
1.0	0.2	0.1121	0.1121	0.1121	1.2871	1.2871	1.2871
1.0	0.0	0	0	0	1.4142	1.4142	1.4142
1.0	0.5	0.2112	0.2112	0.2111	1.1407	1.1408	1.1408

TABLE 2 Shows comparison of the Nusselt number $-\theta'(0)$ and the Sherwood number $-\varphi(0)$ versus M and K of the present study with that of Eldabe et al.[25] and Hsiao[26]

		$-\theta'(0)$			$-\phi'(0)$		
M	K	Ref. [25]	Ref. [26]	Present	Ref. [25]	Ref. [26]	Present
0.0	0.2	0.4688	0.4889	0.4758	0.2149	0.2035	0.2035
0.5	0.2	0.4250	0.4476	0.4375	0.1972	0.1875	0.1875
1.0	0.2	0.3913	0.4159	0.4086	0.1857	0.1770	0.1770
1.0	0.0	0.3734	0.3950	0.3858	0.1790	0.1711	0.1711
1.0	0.5	0.4119	0.4407	0.4267	0.1938	0.1844	0.1844

TABLE 3 The numerical values of $-f''(0)$, $g'(0)$, $-\theta'(0)$ and $-\phi'(0)$ versus K, Pr, E_1, λ

				$Ec = 0.002, n = 0.05, S = 0.1, N = 5, M = 0.01,$ $Nt = Nb = A = Q = \gamma = 0.1, Le = 0.2$			
K	Pr	λ	E_1	$-f''(0)$	$g'(0)$	$-\theta'(0)$	$-\phi'(0)$
0.0	0.2	0.1	0.5	0.5594860	−0.033163	0.31024	0.1659560
0.1	0.3	0.2	0.6	0.1214710	0.0169380	0.40351	0.0992429
0.2	0.5	0.3	0.7	0.1127490	0.0523815	0.49645	−0.047869
0.3	0.5	0.4	0.8	−0.574919	0.0482891	0.59473	−0.035140
0.4	0.6	0.5	0.9	−0.857265	0.0440114	0.67989	−0.092814
0.5	0.7	0.6	1.0	−1.10 7380	0.0315765	0.75760	−0.145082

increment in the thickness of the momentum-boundary layer, while the thickness of the thermal layer decreases.

Figure 8 displays the impact of a chemical reaction parameter γ on fluid velocity, micro-rotation velocity, and concentration behavior. In the case of productive chemical reaction $\gamma > 0$, the concentration behavior of the fluid increases, while an opposite effect is observed when

$\gamma \prec 0$. Moreover, for $\gamma \succ 0$ the angular velocity decreases but the velocity of the nanofluid increase.

Figure 9 shows the effect of modified Hartman number on velocity, angular velocity, and temperature profile. We notice that, increasing the Hartman number values decreases the fluid temperature and microrotation while increase its velocity. This behavior because the Hartman number amplifies the effect of the external and internal forces induced by the applied electric filed.

Figures 10-11 present the flow stream lines in three and two dimensions for different values of the electric field strength. The results showed that the stream lines are concentrated near the stagnation point $x = 0$ when increasing the electric field. While when decreasing the electric field strength the stream lines diverge.

6 | CONCLUSION REMARKS

According to the above results we conclude that:

- The velocity of the boundary layer adjacent to the stretching sheet decreases as the magnetic field parameter increases, but the opposite effect happens for the temperature.
- For $\gamma \succ 0$, the productive chemical reaction increases the fluid concentration, while an opposite effect is observed when $\gamma \prec 0$.
- For a productive chemical reaction near the sheet surface, the angular velocity decreases but opposite trend is observed far from the sheet surface.
- Due to the increase of the mixed convection parameter λ the surface cooling phenomena occurs. This phenomenon occurs as a result of the increases of the fluid velocity, because of the higher value of buoyancy force, and the decreases in the boundary layer thickness.

7 | APPLICATIONS

The present study has very important applications in petroleum engineering, rheology, nuclear reactors, medical fields, and geophysics. Moreover, these results could be used for human blood flow, especially in the case of human cancer treatments.

NOMENCLATURE

$\underline{V}$	fluid velocity
$\underline{J}$	Joule current
n	boundary parameter
$\underline{E}$	electric field
$\underline{B}$	magnetic field
τ_1	the ratio among the efficient heat transfer capacity of the nanoparticles and the fluid heat capacity
μ	kinematic viscosity
ρ_p	particles density
ρ_f	fluid density
σ	electric conducting
Nb	Brownian motion parameter

k_r	thermal conductivity
$(\rho c)_{f,p}$	fluid and nanoparticle material of the heat capacity
D_B	Brownian diffusion coefficient
D_T	thermophoretic coefficient
c	surface stretching constant
T_∞	local temperature
C_o	initial concentration
j	micro inertia density
G_{rx}	local Grashof number
G^*_{rx}	Grashof number due to concentration
λ	mixed convection parameter
j_o	the applied current density in the electrodes
N	the ratio of thermal to concentration buoyancy forces
Q	modified Hartman number
C	concentration of nanoparticles
$\vec{\tau}$	shear stress tensor
$\vec{F}$	force density
s	suction/injection parameter
$\gamma^*, \alpha^*, \beta^*$	spin gradient viscosity coefficient
pr	Prandtl number
u, v	fluid velocity and the normal velocity components in the x and y orientations
E_c	Eckert number
M	Hartmann number
E_1	electric field parameter
R_{ex}	local Reynolds number
N_t	thermophoresis parameter
α	the thermal diffusivity
K	material parameter
β_T, β_C	thermal and mass diffusions coefficients
g	gravity
N_b	Brownian motion parameter
P_r	Prandtl number
L_e	Lewis number
γ	chemical reactions parameter
N^*	component of the microrotation
k_1	vortex viscosity coefficient
υ	kinematic viscosity
M_o	the magnetization of the permanent magnets
T_0	initial temperature
A	dimensionless parameter
a	width for magnets and electrode

REFERENCES

1. Choi SUS, Eastman JA. Enhancing thermal conductivity of fluids with nanoparticles. *ASME Publ Fed*. 1995; 231:99-106.
2. Choi SUS, Zhang ZG, Yu W, Lockwood FE, Grulke EA. Anomalous thermal conductivity enhancement in nanotube suspensions. *Appl Phys Lett*. 2001;79:2252-2254.

3. Reddy MG, Vijayakumari P, Kumar KG, Shehzad SA. Zero-mass flux and Cattaneo–Christov heat flux through a Prandtl non-Newtonian nanofluid in Darcy–Forchheimer porous space. *Heat Transfer*. 2021;50:220-233.
4. Shehzad SA, Reddy MG, Rauf A, Abbas Z. Bioconvection of Maxwell nanofluid under the influence of double diffusive Cattaneo-Christov theories over isolated rotating disk. *Phys Scr*. 2020;95(4):045207.
5. Reddy MG, Padma P, Shankar B. Effects of magnetic field and Ohmic heating on viscous flow of a nanofluid towards a nonlinear permeable stretching sheet. *J Nanofluids*. 2016;5(3):459-470.
6. Eringen AC. Theory of micropolar fluids. *J Math Mech*. 1966;16:1-18.
7. Eringen AC. Theory of thermomicrofluids. *J Math Anal Appl*. 1972;38(2):480-496.
8. Arafa AA, Gorla RSR. Mixed convection boundary layer flow of a micropolar fluid along vertical cylinders and needles. *Int J Eng Sci*. 1992;30:1745-1751.
9. Nadeem S, Rahman A, Vajravel K, Lee J, Lee C. Axisymmetric stagnation flow of a micropolar nanofluid in a moving cylinder. *Math Probl Eng*. 2011:2-18.
10. Bourantas GC, Loukopoulos VC. MHD natural convection flow in a inclined square enclosure filled with a micropolar nanofluid. *Int J Heat Mass Transfer*. 2014;29:930-944.
11. Noor N, Haq FM, Nadeem RUS, Hashim I. Mixed convection stagnation point flow of a micropolar nanofluid along a vertically stretching surface with slip effects. *Mechanica*. 2015;50:2007-2022.
12. Rehman A, Nadeem S. Mixed convection heat transfer in micropolar nanofluid over a vertical slender cylinder. *Chinese Phys Lett*. 2012;29(12):124701.
13. Ram Reedy C, Pradeepa T, Srinivasacharya D. Similarity solution for free convection flow of a micropolar fluid under convective boundary condition via lie scaling group transformations. *Adv High Energy Phys*. 2015;2015:1-16.
14. Besthapu P, Haq RU, Bandari S, Al-Mdallal QM. Mixed convection flow of thermally stratified MHD nanofluid over an exponentially stretching surface with viscous dissipation effect. *J Taiwan Inst Chem Eng*. 2017;71:307-314.
15. Ramzan M, Bilal JD, Chung U. Mixed convective flow of Maxwell nanofluid past a porous vertical stretched surface-an optimal solution. *Results Phys*. 2016;6:1072-1079.
16. Gnaneswara Reddy M, Makinde OD. Magnetohydrodynamic peristaltic transport of Jeffrey nanofluid in an asymmetric channel. *J Mol Liq*. 2016;223:1242-1248.
17. Gnaneswara Reddy M, Rani S. Transverse magnetic flow over a Reiner-Philippoff nanouid by considering solar radiation. *Mod Phys Lett B*. 2019;33(36):1950449.
18. Souayeh B, Gnaneswara Reddy M, Sreenivasulu P, Poornima T, Rahimi-Gorji M, Alarifi IM. Comparative analysis on non-linear radiative heat transfer on MHD Casson nanofluid past a thin needle. *J Mol Liq*. 2019;284:163-174.
19. Rashid I, Haq RU, Al-Mdallal QM. Aligned magnetic field effects on water based metallic nanoparticles over a stretching sheet with PST and thermal radiation effects. *Physca E Low Dimens Syst Nanostruct*. 2017;89:33-42.
20. Eldabe NTM, Gabr ME, Zaher SA. Two dimensional boundary layer flow with heat and mass transfer of magneto hydrodynamic non-Newtonian Nano fluid through porous medium over a semi-infinite moving plate. *Microsyst Technol*. 2018;24:2919-2928.
21. Eldabe NTM, Gabr ME, Zaher SA. The motion of a non-Newtonian Nanofluid over a semi-infinite moving vertical plate through porous medium with heat and mass transfer. *Therm Sci*. 2020;24:1311-1321.
22. Shamshuddin MD, Satya Narayana PV. Combined effect of viscous dissipation and Joule heating on MHD flow past a Riga plate with Cattaneo–Christov heat flux. *Indian J Phys*. 2020;94(9):1385-1394.
23. Buongiorno J. Convective transport in nanofluids. *ASME J Heat Transfer*. 2006;128:240-250.
24. Atif SM, Hussain S, Sagheer M. Numerical study of MHD micropolar carreau nanofluid in the presence of induced magnetic field. *AIP Adv*. 2018;8:035219.

25. Eldabe NTM, Mahmoud E, Ouaf M. Chebyshev finite difference method for heat and mass transfer in a hydromagnetic flow of a micropolar fluid past a stretching surface with Ohmic heating and viscous dissipation. *Appl Math Comput*. 2006;177(2):561-571.
26. Hsiao KL. Micropolar nanofluid flow with MHD and viscous dissipation effects towards a stretching sheet with multimedia feature. *Int J Heat Mass Transfer*. 2017;112:983-990.

How to cite this article: Eldabe NT, Gabr ME, Zaher AZ, Zaher SA. The effect of Joule heating and viscous dissipation on the boundary layer flow of a magnetohydrodynamics micropolar-nanofluid over a stretching vertical Riga plate. *Heat Transfer*. 2021;50:4788–4805. https://doi.org/10.1002/htj.22102